Data based Modelling and Identification of Nonlinear SDOF MOEMS Mirror

David Brunner[a], Han Woong Yoo[a], Thomas Thurner[b], and Georg Schitter[a]

[a]TU Wien, Automation and Control Institute (ACIN), Gusshausstrasse 27-29, 1040 Vienna, Austria
[b]Design Center Graz, Infineon Technologies AG, Babenbergerstrae 10, 8010 Graz, Austria

ABSTRACT

Accurate modeling of MOEMS mirrors is crucial for their design and fabrication, as well as for proper control within its target applications. This paper proposes a novel identification method using a generalized nonlinear SDOF model of an electrostatically actuated 1D resonant MOEMS mirror solely based on measured scanning trajectories and the current generated by the movement of the comb-drive electrodes. The nonlinear stiffness and damping are identified from a decay measurement while the comb-drive torque and the rotor inertia are derived from an actuated decay measurement, where a constant voltage is applied. The simulation with the identified parameters closely matches the measured frequency response including bifurcations and hysteresis. Furthermore a period-based modified index of agreement is proposed for nonlinear systems showing values of over 0.995 at each period along the decay.

Keywords: Micro-Opto-Electro-Mechanical System (MOEMS), Resonant scanning mirror, Data based identification, Generalized nonlinear SDOF model, Actuated decay, Comb-drive torque

1. INTRODUCTION

Resonant micro-opto-electro-mechanical system (MOEMS) mirrors receive much attention in high precision scanning systems since they are cheap, easy to manufacture, allow small form factors, show high performance and low power consumption.[1] For characterization and closed loop control design of the MOEMS mirrors, an accurate model parametrization and estimation is critical to understand and manipulate its most dominant behavior. Although MOEMS designs can have multiple degree of freedom (DOF), the dominant behavior such as scanning motions are usually well separated from other eigenmodes by design, which allows modeling of the device considering only the desired DOFs. Typically the physical parameters of the MOEMS mirror are obtained by finite element simulations as in Ref. 2–5. Model parameter estimation methods based on experimental data are proposed in Ref. 6 and 7, where a given nonlinear analytical model is fitted to the frequency and amplitude data of a ring-down measurement, also called decay. In a similar manner, based on a decay measurement, an estimation method of the effective stiffness and damping ratio of a general nonlinear system is proposed in Ref. 8, where the parameters are identified by assuming a piecewise linear response. The method in Ref. 8 uses the terms of instantaneous amplitude and frequency to extract the nonlinear parameters of the system. However, all those methods provide only a pure mathematical behavioral model describing the so called backbone curve of the system but with no actual physical parameters. Furthermore single harmonic trajectories are assumed while it is in general no exact solution of the equation of motion in the presence of nonlinearities, especially the nonlinear stiffness. Therefore throughout this paper the frequencies are calculated from zero crossings and may not represent a single harmonic oscillation. Additional non-linearity may be introduced by the actuation as in the case of comb-drives, which are electrostatic actuators and show nonlinear voltage and position dependency.[5,9] The comb-drive capacitance and torque curves are usually obtained by an overlap approximation of the comb fingers[5] or by FEM simulations.[10] In case of quasi-static mirrors, the comb-drive torque can be estimated by measuring the static deflection for different applied voltages as in Ref. 2. However the accuracy of this method

Further author information: (Send correspondence to David Brunner)
David Brunner: E-mail: brunner@acin.tuwien.ac.at, Telephone: +43 (0)1 588 01-376 527

Post-print version of the article: D. Brunner, H.W. Yoo, T. Thurner, and G. Schitter, "Data based modelling and identification of nonlinear SDOF MOEMS mirror", *Proc. SPIE 10931*, MOEMS and Miniaturized Systems XVIII, pp. 269 - 278, 2019. DOI: 10.1117/12.2508429

relies on the accuracy of the estimated stiffness and the inertia.

This paper proposes a complete identification of a general nonlinear model of an electrostatically actuated resonant MOEMS mirror solely based on measurement data. First a pure behavioral model including nonlinear stiffness and damping is identified from a decay measurement, where the stiffness is estimated such that the equation of motion is fulfilled by assuming damping to be low. The nonlinear damping is modeled as an amplitude dependent damping coefficient and is identified by matching the dissipated energy to the loss in potential energy in each period. Additionally a possible mathematical realization of the damping behavior in terms of a damping function is given, describing the amplitude dependent damping. After the mechanical behavioral model of the MOEMS mirror is obtained, the electrostatic actuator is analyzed. The nonlinear comb-drive torque is identified by simultaneously measuring the mirror angle and the current through the comb-drive capacitance by an actuated decay. Subsequently the rotor inertia is estimated by matching the dissipated and the injected energy at a specific amplitude point. Finally a comparison of the simulated and the measured response of the MOEMS mirror in time and frequency domain is given.

The proposed modeling and parameter identification technique is demonstrated by a case study on an electrostatically actuated single degree of freedom (SDOF) resonant MOEMS mirror shown in Figure 1. The scanning trajectories are optically measured using a position sensitive detector (PSD) in the test bench proposed in Ref. 11. The frequency response shows a hysteresis between up- and down-sweep as well as bifurcations (jumps), which are well known behavior of such resonators.[12] Due to the characteristics of the comb-drive actuation, the driving frequency is double the mirror frequency. The arrows in the frequency response indicate uni-directional transitions, which cannot be passed in the other direction in a frequency sweep and highly depend on the system parameters.[13] Furthermore this mirror exhibits a hardening behavior with increasing amplitude due to the four leaf springs in addition to the torsional bars. Such structures are usually used to shape the modes of the MOEMS mirror such that the undesired modes are well suppressed. The small angle oscillation frequency of the pure mechanical system, i.e. unactuated mirror, is given by f_{small}. The circuitry used for driving the MOEMS mirror is shown in Figure 2. A MOSFET half-bridge connects the rotor of the MOEMS mirror to a DC high voltage supply or to ground, generating a square wave signal controlled by a single digital input. An additional digital input S_{EN} enables the measurement of the current collected by the stator comb-drive electrodes.

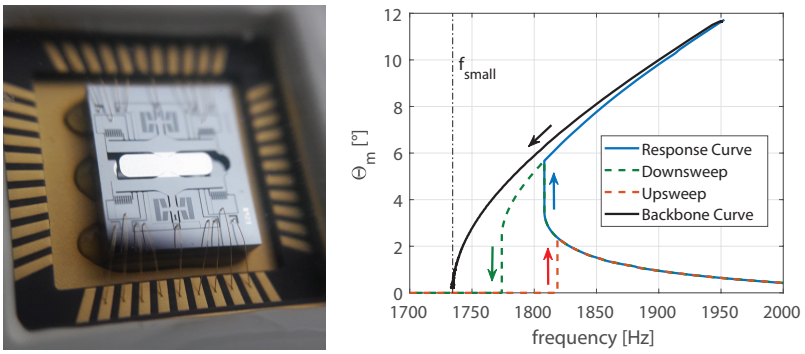

Figure 1. (left) Picture of resonant MOEMS mirror used in this case study. The aluminum coated mirror is of rectangular shape and operated at atmospheric pressure. For safety the whole chip is protected by a glass cover. (right) Measured frequency response, i.e. mechanical amplitude over mirror frequency, by applying a square wave voltage (60V, 50% duty cycle) and backbone curve obtained by a decay measurement. The mirror shows hysteresis and jumps at specific frequencies as well as a hardening behavior with increasing amplitude.

Post-print version of the article: D. Brunner, H.W. Yoo, T. Thurner, and G. Schitter, "Data based modelling and identification of nonlinear SDOF MOEMS mirror", *Proc. SPIE 10931*, MOEMS and Miniaturized Systems XVIII, pp. 269 - 278, 2019. DOI: 10.1117/12.2508429

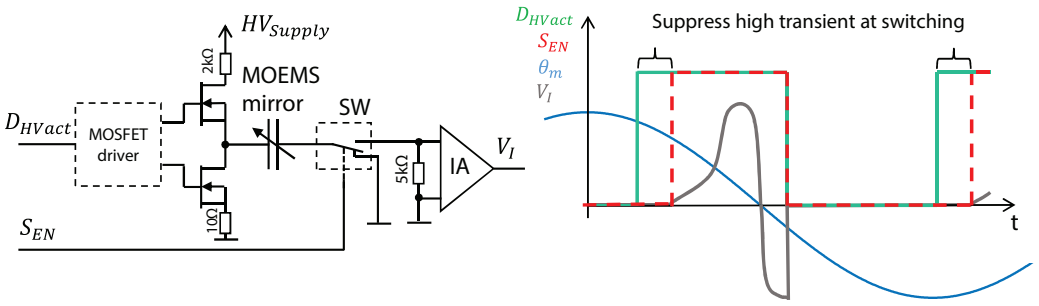

Figure 2. (left) Used MOSFET half-bridge to drive the MOEMS mirror, which is electrically modeled as a variable capacitance, with square wave signals controlled by a single digital input D_{HVact}. The output voltage switches between GND and HV_{Supply}. The input S_{EN} controls the analog switch (SW). The instrumentation amplifier (IA) provides a voltage signal V_I which is proportional to the current through the MOEMS capacitance if S_{EN} is high. (right) Principle signaling example for current sensing. The delayed turning on of S_{EN} is to suppress the high transient current generated by the fast switching of the MOSFETs and to avoid damage of the instrumentation amplifier (IA).

2. NONLINEAR MOEMS MIRROR MODEL IDENTIFICATION

A general model of a SDOF MOEMS mirror is a nonlinear extension of the simple harmonic oscillator (SHO) considering nonlinear functions for the stiffness and the damping[8] as well as for the driving torque. The equation of motion of the MOEMS mirror can be written as

$$J\,\ddot{\theta}_m(t) + \gamma\big(\theta_m(t), \dot{\theta}_m(t)\big)\,\dot{\theta}_m(t) + k\big(\theta_m(t)\big)\,\theta_m(t) = \tau_{comb}\big(t, \theta_m(t)\big)\,, \tag{1}$$

which allows arbitrary stiffness $k\big(\theta_m(t)\big)$ and damping coefficient functions $\gamma\big(\theta_m(t), \dot{\theta}_m(t)\big)$, while a constant inertia J is assumed. The actuation torque τ_{comb} of the comb-drive is a function of the mechanical mirror angle $\theta_m(t)$ and the applied voltage $V(t)$ as

$$\tau_{comb}\big(t, \theta_m(t)\big) = \frac{1}{2}\frac{\mathrm{d}C\big(\theta_m(t)\big)}{\mathrm{d}\theta_m} V^2(t)\,, \tag{2}$$

where $C\big(\theta_m(t)\big)$ is the angle dependent comb-drive capacitance.

2.1 MECHANICAL BEHAVIORAL MODEL

For the estimation of the mechanical parameters in the left side of Equation (1), the mirror is driven to a high amplitude and the decay is measured by turning off the actuation as shown in Figure 3. The amplitude over frequency behavior of the mirror trajectory $\theta_m(t)$ follows the backbone curve in the right side of Figure 1, representing the pure mechanical behavior of the mirror.

Since the unactuated mirror model in Equation (1) is not explicit and can be scaled by the inertia J, it is normalized by arbitrarily set $J = 1\,kg\,m^2$ and normalized parameters are marked with a prime. This leads to a normalized mechanical equation of motion as

$$\ddot{\theta}_m(t) + \gamma'\big(\theta_m(t), \dot{\theta}_m(t)\big)\,\dot{\theta}_m(t) + k'\big(\theta_m(t)\big)\,\theta_m(t) = 0\,. \tag{3}$$

The obtained backbone curve in Figure 1 clearly shows a nonlinear stiffening of the mirror and furthermore the right side in Figure 3 indicates a nonlinear energy dissipation as also proposed in Ref. 7. The characteristics of a SHO at a decay measurement are a constant oscillation frequency and an exponentially decreasing envelope described by a single exponential term. However at the presence of any non-linearity this simplified model is no

Post-print version of the article: D. Brunner, H.W. Yoo, T. Thurner, and G. Schitter, "Data based modelling and identification of nonlinear SDOF MOEMS mirror", *Proc. SPIE 10931*, MOEMS and Miniaturized Systems XVIII, pp. 269 - 278, 2019. DOI: 10.1117/12.2508429

longer valid. For example a system with linear damping and nonlinear stiffness already leads to envelopes that cannot be fitted by only one exponential term and therefore this criteria can only be used as an indicator for nonlinear damping.

However at low amplitudes, the mirror response becomes almost linear, i.e. the frequency is rather constant and the envelope can be fitted by a single exponential function, i.e. $\alpha_1\, e^{-\beta_1 t}$. Therefore the linear stiffness and damping coefficient can be estimated by analyzing the small angle response and are derived by $k'_{small} = (2\pi f_{small})^2$ and $\gamma'_{small} = 2\beta_1$.

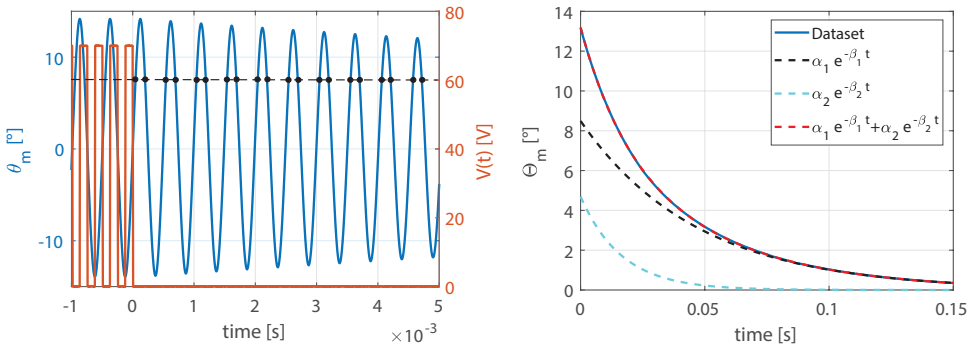

Figure 3. (left) Measured decay trajectory and driving signal. The decay is initiated by keeping the actuation voltage zero. The black dots illustrate an exemplary dataset for the evaluation of Equation (4) at a mechanical angle of 7.5°, given by a dashed line. (right) Decay envelope over time and its exponential function fits. The sum of two exponential functions is necessary to properly fit the envelope over the whole decay, indicating the presence of nonlinear energy dissipation.

Since typical MOEMS mirrors have high Q factors, the torque generated by the springs is much higher than the damping torque except at low angles. Therefore, it can be assumed that the non-constant terms of the damping coefficient do not contribute much to the local force balance at each angular deflection. So the nonlinear stiffness function can theoretically be estimated by simply evaluating the equation of motion given in Equation (3) at each point of the decay. In order to cope with measurement noise, while providing enough bandwidth for accurate trajectory reconstruction, the signal of the decay measurement is filtered by a low pass zero phase filter with bandwidth of 12 kHz. In addition, $\ddot{\theta}_m$ and $\dot{\theta}_m$ are grouped for constant angle θ_m and the corresponding equivalent stiffness k' is estimated by solving the least square problem

$$\min_{k'} \left\| \ddot{\boldsymbol{\theta}}_{\boldsymbol{m}} + \gamma'_{small}\, \dot{\boldsymbol{\theta}}_{\boldsymbol{m}} + k'\, \boldsymbol{\theta}_{\boldsymbol{m}} \right\|_2^2 , \tag{4}$$

where $\ddot{\boldsymbol{\theta}}_{\boldsymbol{m}}$, $\dot{\boldsymbol{\theta}}_{\boldsymbol{m}}$ and $\boldsymbol{\theta}_{\boldsymbol{m}}$ are $n\times 1$ vectors containing the dataset values where the mirror hits θ_m. Since the velocity is shifted in phase regarding the deflection, while the acceleration has just inverse sign, the influence of damping on Equation (4) is even further reduced by the use of positive and negative transitions of the evaluated angle points as indicated in the left side of Figure 3. Noise sensitivity is further reduced by imposing that the stiffness has to be symmetric in θ_m, i.e. $k'(\theta_m) = k'(-\theta_m)$. The evaluation of Equation (4) provides an estimated k' value for each angular position, which is shown in Figure 4, where also the corresponding spring torque $\tau'_{sp} = k'\,\theta_m$ is shown. Since the stiffness function is forced to be symmetric, the spring torque is consequently asymmetric in θ_m. The obtained curves are fitted by polynomial functions, which are used in the following analysis.

Damping models of MOEMS mirrors are still content of extensive research[7,14,15] and highly depend on the geometry and the pressure range where they are operated. As the damping torque is very low, it is difficult to estimate it at every time instance of the decay measurement. Therefore, the nonlinear damping is approximated

Post-print version of the article: D. Brunner, H.W. Yoo, T. Thurner, and G. Schitter, "Data based modelling and identification of nonlinear SDOF MOEMS mirror", *Proc. SPIE 10931*, MOEMS and Miniaturized Systems XVIII, pp. 269 - 278, 2019. DOI: 10.1117/12.2508429

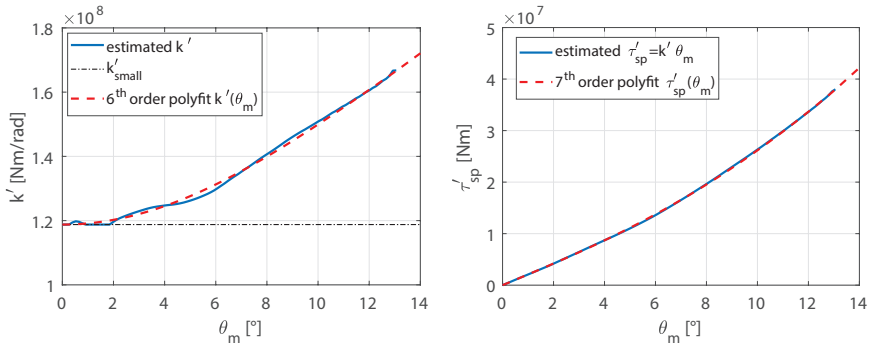

Figure 4. Estimated normalized spring stiffness (left) and torque (right) function over the mirror mechanical angle obtained by evaluating Equation (4). The estimated values are fitted by a polynomial function using *polyfit* in MATLAB.

by calculating an averaged damping coefficient γ'_i for each mirror period along the decay and assume it is a function of the mirror amplitude Θ_m. This allows to model any non-linearity in the damping coefficient provided that it is relatively small and a sufficiently smooth function of the mirror amplitude.

The averaged damping coefficient can be obtained by calculating the potential energy loss in the spring from each amplitude to the next along the decay. This corresponds to the normalized dissipated energy per cycle E'_d in Figure 5 and can be written as

$$E'_d(\Theta_{m,i}) = \gamma'_i \int_{\theta_m(t_i)}^{\theta_m(t_{i+1})} \dot{\theta}_m(t)\, \mathrm{d}\theta_m \,, \tag{5}$$

where i denotes the i^{th} period. Figure 6 shows the calculated damping coefficient over the mirror amplitude. The corresponding Q factor is then calculated by $Q = 2\pi \frac{E'_{pot}(\Theta_{m,i})}{E'_d(\Theta_{m,i})}$, where $E'_{pot}(\Theta_{m,i})$ denotes the potential energy stored in the spring at the beginning of the period and is shown at the right side in Figure 6. The limited measurement SNR leads to noisy estimations at low mirror amplitudes. However the small amplitude values γ'_{small} and $Q_{small} = \frac{2\pi f_{small}}{\gamma'_{small}}$ are known from the previous analysis and have to be reached asymptotically.

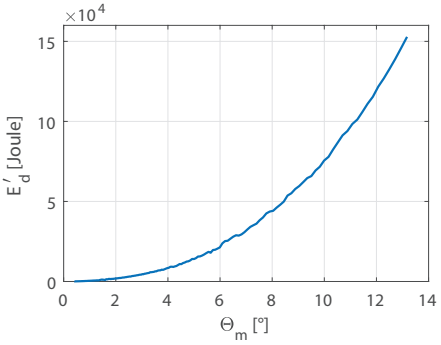

Figure 5. Normalized dissipated energy per mirror period over amplitude. This energy correspond to the potential energy difference of adjacent amplitudes in the decay measurement.

Post-print version of the article: D. Brunner, H.W. Yoo, T. Thurner, and G. Schitter, "Data based modelling and identification of nonlinear SDOF MOEMS mirror", *Proc. SPIE 10931*, MOEMS and Miniaturized Systems XVIII, pp. 269 - 278, 2019. DOI: 10.1117/12.2508429

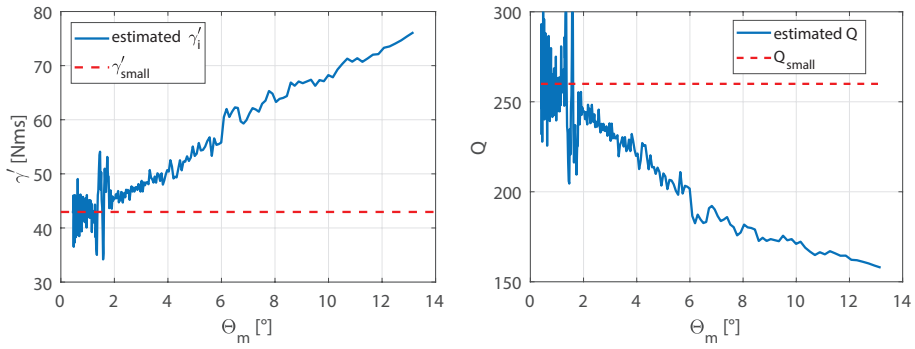

Figure 6. (left) Amplitude dependent normalized damping coefficient γ' of the individual periods extracted from the decay measurement using Equation (5). The estimation gets noisy at low amplitudes due to the limited measurement SNR. (right) Corresponding Q factor dependency. It is shown that even in normal pressure condition the MOEMS mirror has a high Q factor which generally depends on the operation amplitude.

2.2 REALIZATION OF DAMPING FUNCTION

In order to use the identified amplitude dependent normalized damping coefficient γ'_i in the mirror model, the current amplitude has to be known at each time step. This can be implemented by introducing an arbitrary function which unambiguously maps the amplitude to a value that can be calculated at each time from the current states. In this study a function h is used, which represents the amplitude state by the low-pass filtered angular velocity squared and is shown in the left side of Figure 7. By using the decay measurement data, the amplitude dependent normalized damping coefficient γ'_i at each period can be substituted by the h-dependent function $\gamma'_h(h)$ as shown in the right side of Figure 7.

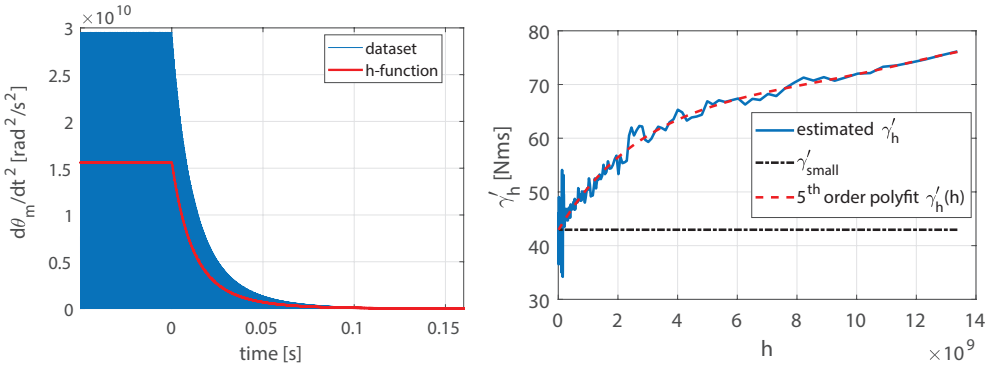

Figure 7. (left) Angular velocity squared of decay measurement and ideal h-function obtained by using the $filtfilt$-function in MATLAB. (right) Corresponding h dependent normalized damping coefficient where the amplitude of each period is mapped into the function h.

The normalized mechanical model is then completed as

$$\ddot{\theta}_m(t) + \gamma'_h\big(h(t)\big)\,\dot{\theta}_m(t) + k'\big(\theta_m(t)\big) = 0 \tag{6}$$

$$\frac{1}{\omega_c^2}\,\ddot{h}(t) + \frac{2\xi}{\omega_c}\,\dot{h}(t) + h(t) = \dot{\theta}_m^2\,, \tag{7}$$

where a second order low-pass filter ($\omega_c = 2\pi 800\frac{1}{s}$ and $\xi = 1$) is used to obtain the corresponding h value for the damping coefficient selection. Since $\dot{\theta}_m^2$ has doubled mirror frequency (i.e. $> 3400\,\text{Hz}$), a filter bandwidth of

Post-print version of the article: D. Brunner, H.W. Yoo, T. Thurner, and G. Schitter, "Data based modelling and identification of nonlinear SDOF MOEMS mirror", *Proc. SPIE 10931*, MOEMS and Miniaturized Systems XVIII, pp. 269 - 278, 2019. DOI: 10.1117/12.2508429

800 Hz is a good tradeoff between high frequency suppression and fast tracking of the mirror amplitude, needed at a decay simulation.

2.3 COMB-DRIVE TORQUE AND CAPACITANCE

As given in Equation (2) the comb-drive torque is proportional to the derivative of the comb-drive capacitance with respect to the deflection angle θ_m. The capacitance derivative can be calculated by measuring the current through the comb-drive and the mirror angle simultaneously. The proposed method is performing an actuated decay, where the actuation is a constant voltage (i.e. $\frac{\mathrm{d}V}{\mathrm{d}t} = 0$) and integrates the measured current ($I(\theta_m) = V\frac{\mathrm{d}C(\theta_m)}{\mathrm{d}t}$) generated by the mirror movement over a full mirror period as can be seen in the left side of Figure 8. Using the equation

$$C\big(\theta_m(t)\big) = \int_{t_{start}}^{t_{end}} \frac{C\big(\theta_m(t)\big)}{dt}\mathrm{d}t + const. = \int_{t_{start}}^{t_{end}} \frac{I\big(\theta_m(t)\big)}{V}\mathrm{d}t + const.\,, \tag{8}$$

the capacitance and subsequently the comb-drive torque curve are estimated as a function of the mirror angle. Since only the relative changes and not the absolute values of the capacitance are of interest, the capacitance function can be arbitrarily set to $\Delta C(\theta_m) = C(\theta_m) - C(0)$. The results are shown at the right side of Figure 8, where the comb-drive torque is divided by the voltage squared to provide a voltage independent value. This method extracts the actual capacitance variation and torque curve of the MOEMS mirror during operation accounting for all parasitic effects such as the fringing fields with only one measurement.

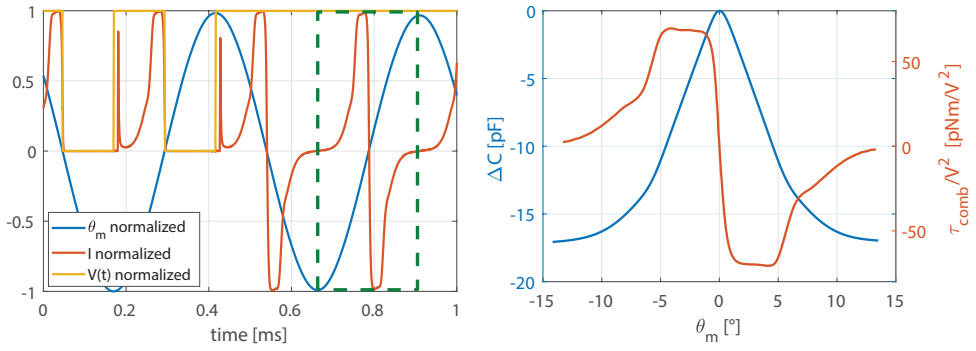

Figure 8. (left) Decay measurement with constant voltage (actuated decay) and data extraction window, i.e. t_{start} to t_{end}, shown in green dashed rectangle. (right) Extracted capacitance change and comb-drive torque over mirror angle. The torque can be easily calculated by taking the derivative of the capacitance and is here normalized by the applied voltage squared.

2.4 ROTOR INERTIA

To derive a full model of the MOEMS mirror, the normalized mechanical parameters derived in Sec. 2.1 have to be rescaled in order to match the actual physical parameters. This scaling factor represented by the rotor inertia J can be estimated by matching the injected energy to the dissipated energy within one period at a steady state oscillation. Assuming a synchronized driving condition, i.e. the voltage $V(t)$ is switched off at zero crossing of the mirror and switched on at the amplitude point, the injected energy per driving period is

$$E_C(\Theta_m) = \int_{\Theta_m}^{0} \frac{1}{2}V^2\frac{\mathrm{d}C(\theta_m)}{\mathrm{d}\theta_m}\,\mathrm{d}\theta_m = \frac{1}{2}V^2\big(0 - \Delta C(\Theta_m)\big)\,, \tag{9}$$

where Θ_m is the obtained maximum deflection amplitude for a specific voltage V and ΔC is the capacitance function obtained in the previous section.

Post-print version of the article: D. Brunner, H.W. Yoo, T. Thurner, and G. Schitter, "Data based modelling and identification of nonlinear SDOF MOEMS mirror", *Proc. SPIE 10931*, MOEMS and Miniaturized Systems XVIII, pp. 269 - 278, 2019. DOI: 10.1117/12.2508429

From the decay measurement in Sec. 2.1, the dissipated energy per mirror period for each amplitude is known and given in Figure 5. Since E_C is an unscaled energy and it is injected two times per mirror period, the inertia J can be calculated by

$$J = \frac{2\,E_C(\Theta_m)}{E_d'(\Theta_m)} = 4.868 \cdot 10^{-13} kg\,m^2\,. \tag{10}$$

This assumes that the actuation does not significantly change the mirror trajectory and therefore the energy dissipation, which usually holds for such high Q systems driven in resonance.

The identification of the full MOEMS mirror model including also the actuation term is now completed as

$$\ddot{\theta}_m(t) + \gamma_h'\big(h(t)\big)\,\dot{\theta}_m(t) + k'\big(\theta_m(t)\big) = \frac{1}{J}\tau_{comb}(t,\theta_m) \tag{11}$$

$$\frac{1}{\omega_c^2}\,\ddot{h}(t) + \frac{2\xi}{\omega_c}\,\dot{h}(t) + h(t) = \dot{\theta}_m^2\,. \tag{12}$$

The actual physical stiffness and damping coefficients can be easily calculated by $k(\theta_m) = J\,k'(\theta_m)$ and $\gamma_h(h) = J\,\gamma_h'(h)$ respectively, while the Q factor and the h function are not effected by the normalization.

3. MODEL VALIDATION

In this section the identified MOEMS mirror model is simulated in MATLAB Simulink and compared to the measured data. Figure 9 shows a comparison of simulated and measured decay response of the mirror (i.e. $\tau_{comb} = 0$). For model validation of linear systems in time domain, the modified index of agreement d_1[16–18] can be used, which allows a phase and amplitude error sensitive comparison of trajectories.[19] However in contrast to linear systems, the frequency varies along the decay and a small frequency error would accumulate to a large phase error as the time passes, resulting in a low agreement value and misleading the performance of the identified model. Therefore a period-based modified index of agreement is proposed as

$$d_1(i) = 1 - \frac{\sum_k^{N(i)} |\theta_i(k) - \hat{\theta}_i(k)|}{\sum_k^{N(i)} |\theta_i(k) - \bar{\theta}_i| + |\hat{\theta}_i(k) - \bar{\theta}_i|} \tag{13}$$

where θ_i and $\hat{\theta}_i$ denote measurement and simulation of mechanical mirror angles during i-th period from the start of decay, respectively. $\bar{\theta}_i$ is the average value of the measured mechanical mirror angle at i-th period. The evaluation size $N(i)$ consists of the zero-crossings at start and end of the i-th period as well as all measured sample points in between. The simulation data of i-th period is shifted in time to match the corresponding start zero-crossing of the measurement and is interpolated at the times corresponding to the measured sample points to obtain $\hat{\theta}_i(k)$. The right side of Figure 9 illustrates the period-based modified index of agreement along the decay measurement showing that the derived model fits the measured data with an modified index of agreement of at least 0.995 at each period in this case study.

Figure 10 shows the simulation of the frequency response and a comparison to the measurements. The mismatch at low amplitudes and high frequency is subject of further investigation. Besides the simulation results closely match the measured amplitude over frequency behavior of the MOEMS mirror. The derived model also shows hysteresis and bifurcations, which accurately match to the measurement even though the model parameters are identified solely from a decay and an actuated decay measurement data.

The identified MOEMS mirror model shows a good agreement in time and frequency domain and provides physical parameters of the system. This enables MOEMS designers to prove their simulations and also manufacturers to accurately detect variations in all system parameters separately. Furthermore the model can be easily used for closed loop control design and stability analysis.

Post-print version of the article: D. Brunner, H.W. Yoo, T. Thurner, and G. Schitter, "Data based modelling and identification of nonlinear SDOF MOEMS mirror", *Proc. SPIE 10931*, MOEMS and Miniaturized Systems XVIII, pp. 269 - 278, 2019. DOI: 10.1117/12.2508429

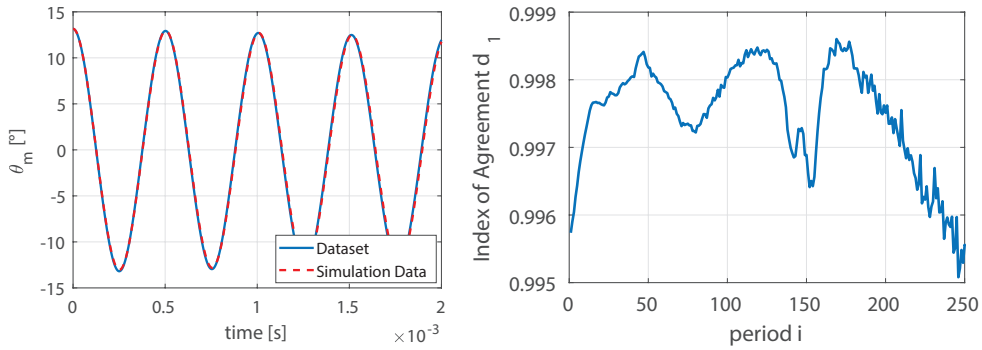

Figure 9. (left) Decay trajectory comparison of simulation and measured data. Only about first four periods are shown for clarity of the trajectories. (right) Index of agreement calculated for each individual period. The accumulated phase error is compensated by shifting the trajectory of each period in time such that the first zero crossings match.

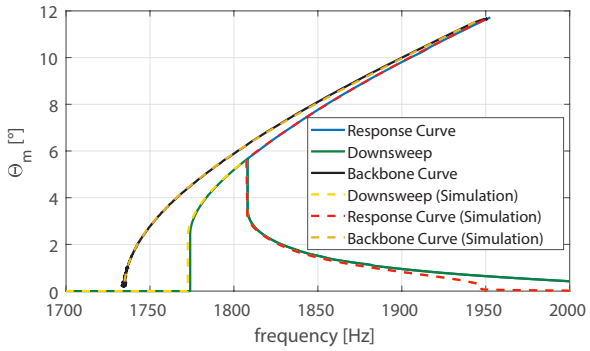

Figure 10. Measured and simulated frequency response of MOEMS mirror. The derived model closely matches the measured response and shows the same characteristic hysteresis and jumps at the same driving conditions (i.e. 60V, 50% duty cycle).

4. CONCLUSION

An identification method for a generalized nonlinear SDOF model is proposed to characterize a SDOF resonant MOEMS mirror, without need of prior knowledge on the used modeling parameters but solely measurement data. Since even at atmospheric pressure, resonant MOEMS mirrors have Q factors in the range of several hundreds, the nonlinear stiffness is estimated by neglecting the damping nonlinearities and solving a least square problem at each mechanical mirror angle of a decay measurement. Subsequently the nonlinear damping is approximated by averaged damping coefficients for each period, which are assumed to be amplitude dependent. As a realization of the identified damping behavior a function h is introduced, which represents the amplitude state. The comb-drive capacitance and torque are estimated by a simultaneous measurement of the angle and the current through the comb-drives by an actuated decay. This method provides an accurate identification of the actuation torque without any additional knowledge of the system and represent real physical values. By a synchronized driving of the mirror and matching of injected and dissipated energy, the rotor inertia is calculated to $J = 4.868 \cdot 10^{-13} kg\,m^2$, which enables a full response simulation of the mirror. The derived nonlinear model is verified in time domain by introducing a period-based modified index of agreement which results in values of over 0.995 at each period. The frequency response also shows a close match especially at the bifurcations, which are never considered in the identification.

As next steps, the proposed identification method of the MOEMS mirror can be further optimized and more

Post-print version of the article: D. Brunner, H.W. Yoo, T. Thurner, and G. Schitter, "Data based modelling and identification of nonlinear SDOF MOEMS mirror", *Proc. SPIE 10931*, MOEMS and Miniaturized Systems XVIII, pp. 269 - 278, 2019. DOI: 10.1117/12.2508429

detailed analysis of the mirror behavior can be done. Furthermore the MOEMS mirror model can be used in order to derive control strategies that enable stable and accurate scanning, even at harsh environmental conditions.

ACKNOWLEDGMENTS

This work has been supported in part by the Austrian Research Promotion Agency (FFG) under the scope of the LiDcAR project (FFG project number 860819).

REFERENCES

[1] Thakur, R., "Scanning lidar in advanced driver assistance systems and beyond: Building a road map for next-generation lidar technology," *IEEE Consumer Electronics Magazine* **5**(3), 48–54 (2016).

[2] Schroedter, R., Sandner, T., Janschek, K., Roth, M., and Hruschka, C., "Real-time closed-loop control for micro mirrors with quasistatic comb drives," *Proc.SPIE* **9760**, 9760 – 9760 – 13 (2016).

[3] Chen, C., Zanette, D. H., Guest, J. R., Czaplewski, D. A., and López, D., "Self-sustained micromechanical oscillator with linear feedback," *Phys. Rev. Lett.* **117**, 017203 (2016).

[4] Hung, A. C.-L., Lai, H. Y.-H., Lin, T.-W., Fu, S.-G., and Lu, M. S.-C., "An electrostatically driven 2d micro-scanning mirror with capacitive sensing for projection display," *Sensors and Actuators A: Physical* **222**, 122 – 129 (2015).

[5] Izawa, T., Sasaki, T., and Hane, K., "Scanning micro-mirror with an electrostatic spring for compensation of hard-spring nonlinearity," *Micromachines* **8**, 240 (2017).

[6] Polunin, P. M., Yang, Y., Dykman, M. I., Kenny, T. W., and Shaw, S. W., "Characterization of mems resonator nonlinearities using the ringdown response," *Journal of Microelectromechanical Systems* **25**(2), 297–303 (2016).

[7] Nabholz, U., Heinzelmann, W., Mehner, J. E., and Degenfeld-Schonburg, P., "Amplitude- and gas pressure-dependent nonlinear damping of high-q oscillatory mems micro mirrors," *Journal of Microelectromechanical Systems* **27**(3), 383–391 (2018).

[8] Londoo, J. M., Neild, S. A., and Cooper, J. E., "Identification of backbone curves of nonlinear systems from resonance decay responses," *Journal of Sound and Vibration* **348**, 224 – 238 (2015).

[9] Elshurafa, A. M., Khirallah, K., Tawfik, H. H., Emira, A., Aziz, A. K. S. A., and Sedky, S. M., "Nonlinear dynamics of spring softening and hardening in folded-mems comb drive resonators," *Journal of Microelectromechanical Systems* **20**(4), 943–958 (2011).

[10] Ataman, C. and Urey, H., "Modeling and characterization of comb-actuated resonant microscanners," *Journal of Micromechanics and Microengineering* **16**(1), 9 (2006).

[11] Yoo, H. W., Druml, N., Brunner, D., Schwarzl, C., Thurner, T., Hennecke, M., and Schitter, G., "Mems-based lidar for autonomous driving," *e & i Elektrotechnik und Informationstechnik* **135**(6), 408–415 (2018).

[12] Antonio, D., Zanette, D. H., and Lpez, D., "Frequency stabilization in nonlinear micromechanical oscillators," *Nature communications* (2012).

[13] Kumar, V., Yang, Y., Boley, J. W., Chiu, G. T. ., and Rhoads, J. F., "Modeling, analysis, and experimental validation of a bifurcation-based microsensor," *Journal of Microelectromechanical Systems* **21**(3), 549–558 (2012).

[14] Pandey, A. K., Pratap, R., and Chau, F. S., "Effect of pressure on fluid damping in mems torsional resonators with flow ranging from continuum to molecular regime," *Experimental Mechanics* **48**(1), 91–106 (2008).

[15] Russell, F., Barnaby, P., Ivan, G., Duncan, C., Owen, C., Joseph, M., and E, G., "Air damping analysis in resonating micro-mirrors," 1–5 (2018).

[16] Garrick, M., Cunnane, C., and Nash, J. E., "A criterion of efficiency for rainfall-runoff models," *Journal of Hydrology* **36**(3), 375–381 (1978).

[17] Willmott, C. J., Ackleson, S. G., Davis, R. E., Feddema, J. J., Klink, K. M., Legates, D. R., O'Donnell, J., and Rowe, C. M., "Statistics for the evaluation and comparison of models," *Journal of Geophysical Research: Oceans* **90**(C5), 8995–9005 (1985).

[18] Legates, D. R. and McCabe, G. J., "Evaluating the use of goodness-of-fit Measures in hydrologic and hydroclimatic model validation," *Water Resources Research* **35**(1), 233–241 (1999).

Post-print version of the article: D. Brunner, H.W. Yoo, T. Thurner, and G. Schitter, "Data based modelling and identification of nonlinear SDOF MOEMS mirror", *Proc. SPIE 10931*, MOEMS and Miniaturized Systems XVIII, pp. 269 - 278, 2019. DOI: 10.1117/12.2508429

[19] Muroi, H. and Adachi, S., "Model validation criteria for system identification in time domain," *IFAC-PapersOnLine* **48**(28), 86 – 91 (2015). 17th IFAC Symposium on System Identification SYSID 2015.